AUTHOR QUERY FORM

Dear Author,

Below are the queries associated with your article; please answer all of these queries before sending the proof back to AIP. Author please indicate the correct color processing option from the list below:

1. Author, please confirm Figure number(s) that should appear as color in print. Please know that a fee of $325 per figure will apply for figures printed in color.
2. Author, please confirm Figure number(s) that should appear as color online only, there will be no fees applied.
3. Author, your paper currently does not include any color figures for online or print. If color is needed please indicate which figures it should be applied to and whether it is color in print or online.

Article checklist: In order to ensure greater accuracy, please check the following and make all necessary corrections before returning your proof.

1. Is the title of your article accurate and spelled correctly?
2. Please check affiliations including spelling, completeness, and correct linking to authors.
3. Did you remember to include acknowledgment of funding, if required, and is it accurate?

Location in article	Query / Remark: click on the Q link to navigate to the appropriate spot in the proof. There, insert your comments as a PDF annotation.
Q1	Please check that the author names are in the proper order and spelled correctly. Also, please ensure that each author's given and surnames have been correctly identified (given names are highlighted in red and surnames appear in blue).
Q2	Please provide department names in affiliations 1 and 4.
Q3	Please provide city, state, and zip code details for affiliation 2.
Q4	Please provide the keywords for this article.
Q5	Readers of print will only see figures in black and white. Please modify your text in the caption of Fig. 6 accordingly.
Q6	The resolution of Fig. 6 is low. If you are not satisfied with the way the figure appears in the proof, please provide a new figure file of higher resolution.
	Please check and confirm the Funder(s) and Grant Reference Number(s) provided with your submission: LANL/UCSB, IMMS program European Commision, ITN "Supolen", FP7-607937 European Commision, Horizon 2020-INFRAIA-2016-1, EUSMI project no. 7310219 Please add any additional funding sources not stated above:

Thank you for your assistance.

Microstructural characterization of a star-linear polymer blend under shear flow by using rheo-SANS

L. T. Andriano,[1] N. Ruocco,[1,a)] J. D. Peterson,[1] D. Olds,[2,3] M. E. Helgeson,[1] K. Ntetsikas,[4] N. Hadjichristidis,[4] S. Costanzo,[5] D. Vlassopoulos,[5] R. P. Hjelm,[3] and L. G. Leal[1,b)]

[1] ■ *University of California Santa Barbara, Santa Barbara, California 93106-5080*
[2] *National Synchrotron Light Source II, Brookhaven National Laboratory,* ■, ■ ■
[3] *National Security Education Center, Los Alamos National Laboratory, New Mexico Consortium, Los Alamos, New Mexico 87545*
[4] *■, King Abdullah University of Science and Technology, Thuwal 23955, Saudi Arabia*
[5] *Institute of Electronic Structure and Laser, Department of Materials Science and Technology and FORTH, University of Crete, 70013 Heraklion, Crete, Greece*

Abstract

We present an investigation into the dynamic relaxation mechanisms of a polybutadiene blend composed of a four-arm star (10 wt. %) and a linear polymer matrix in the presence of an applied shear flow. Our focus was the response of the star polymer, which cannot be unambiguously assessed via linear viscoelastic measurements since the signature of the star polymer can barely be detected due to the dominant contribution of the linear matrix. By utilizing small-angle neutron scattering (SANS) coupled with a Couette shear device and a deuterated matrix polymer, we investigated the dynamics of the minority star component of the blend. Our results confirm that the stars deform anisotropically with an increasing shear rate. We have compared the SANS data with predictions from the well-established scattering adaptation of the state-of-the-art tube model for entangled linear polymer melts undergoing shear, i.e., Graham, Likhtman, Milner, and McLeish (GLaMM) approach, appropriately modified following earlier studies in order to apply to the star. This modified model, GLaMM-R, includes the physics necessary to understand stress relaxation in both the linear and nonlinear flow regimes, i.e., contour length fluctuations, constraint release, convective constraint release, and chain retraction. The full scattering signal is due to the minority star component and, although the contribution of the linear chains is hidden from the neutron scattering, they still influence the star polymer molecular dynamics, with the applied shear rate ranging from approximately 8 to 24 s^{-1}, below the inverse relaxation time of the linear component. This study provides another confirmation that the combination of rheology and neutron scattering is an indispensable tool for investigating the nonlinear dynamics of complex polymeric systems. © 2020 The Society of Rheology. https://doi.org/10.1122/1.5121317

I. INTRODUCTION AND THEORETICAL BACKGROUND

Over the past decade, new applications and processing methods have led to a renewed interest in the mechanical properties of polymer blends comprising both linear and branched architectures [1–11]. There is both a practical and theoretical interest in understanding how the properties of a linear polymer matrix might be altered via blending with a small amount of polymer possessing a different, well-defined, complex architecture. An enormous advantage would be gained, for example, if there were a predictable recipe for blending polymers of different well-defined complex architectures to achieve and optimize mechanical properties of a polymer melt, e.g., extension hardening [12–21].

An active area of research for polymer solutions and melts containing both branched and linear polymers is to understand how the presence of a linear chain matrix influences the relaxation of branched chains. In the linear viscoelastic regime, significant progress has been made and different theoretical models describe accurately the effects of adding branched polymers into a linear matrix [7–10]. Actually, a recent study by Hall *et al.* has shown that when the linear polymer has a relaxation time longer than the star component, the terminal relaxation time dependence has nonmonotonic dependence on the blend composition, and this result is obtained both theoretically and experimentally [11]. However, in the nonlinear flow regime (relevant to industrial processing conditions), the theoretical understanding of this problem is still in its infancy, and conventional rheological techniques are not always well suited for probing the response of branched polymers, especially when their fraction is small [22–25].

The tool necessary to predict both molecular scale structure and macroscopic flow in realistic processing configurations is a quantitatively accurate microscopic theory. The macroscopic properties of a bulk polymer in the fluid state depend on the chain configurations and their modification in flow, and these, in turn, depend on the topological interactions between the polymer molecules. The primary topological effect in concentrated solutions or melts is the entanglements, namely, the

---

a)Present address: ExxonMobil Chemical Company, Baytown Technology and Engineering Complex, Baytown, TX 77520.

b)Author to whom correspondence should be addressed. ~~Fax: +1 (805) 893–5458.~~ Electronic mail: lgl20@engr.ucsb.edu

long-lived topological constraints that form a physical network that hinders the chains from translating normal to one another, thus impacting their dynamics [26–29].

The most significant advance in the field was the tube model theory developed originally by de Gennes, Doi, and Edwards [28,29] and subsequently improved to provide more accurate predictions of the linear and in part nonlinear visco-elastic behavior, based on the molecular characteristics of entangled polymers, mainly molar mass, plateau modulus, and Rouse time of an entanglement segment [4,14–16,19,30]. Although the tube model was originally intended to describe entangled melts (or solutions) of monodisperse, linear polymers, it has since been successfully extended to polydisperse linear chain melts [19,31,32] and complex macromolecular architectures [33–36]. However, at present, the understanding of (linear and nonlinear) dynamics of mixed architectures (branched and linear polymers) remains an open issue, as will be discussed below.

According to the tube model, topological constraints in the surrounding environment restrict the lateral motion of a polymer chain but not its curvilinear motion. To the extent that the polymer chain has some limited freedom for lateral motion, the complexities of the surrounding topological environment can be replaced by a smooth tubelike structure [26–29]. The polymer cannot pass through the tube walls (which are not fixed in reality, as discussed below), but it is free to fluctuate within this tube by Rouse-like rearrangements of its configuration. Rearrangements taking place over distances comparable to the tube diameter occur very fast, on a time scale τ_e (Rouse relaxation time of an entanglement segment). Rearrangements within the tube taking place over distances comparable to the full chain contour length are slower, taking a chain Rouse time $\tau_R = Z^2 \tau_e$, where Z is the number of entanglements per chain. To fully relax its stress, the polymer must evacuate the tube via different mechanisms, namely, curvilinear diffusion (reptation), contour length fluctuation (CLF), thermal or convective constraint release (TCR/CCR), and constraint release Rouse (CRR) relaxation [3,19,28,37]. The characteristic time scale for relaxation by reptation is $\tau_{d,\mathrm{lin}} = 3Z^3 \tau_e$. Depending on the details of the polymer architecture and the applied deformation (linear or nonlinear), the relaxation processes (CLF, TCR/CCR, and CRR) may play an important, or in some cases a dominant, role.

CLFs reflect the fact that chain ends can escape the confining tube (and thereby relax the associated stress) as they fluctuate back toward their preferred unstretched contour length [14–26]; it also applies to star arms that do not reptate. TCR and CCR are complementary mechanisms that account for the release of entanglements due to Brownian or externally induced motion of chains, respectively. When a constraint is removed by reptation or CLF, we have TCR, since reptation and CLF are driven by thermal fluctuations. When a constraint is removed by convection due to flow, CCR takes place [19,30,38,39]. CRR relaxation is the mechanism by which stress relaxes following TCR or CCR. When TCR and CCR are present, the tube is better described as a fluctuating field instead of a fixed object. To a first approximation, one expects that CRR and TCR allow the whole tube to undergo the same kind of Rouse-like rearrangements but on a much longer time scale than the Rouse time, τ_R. In the present work, we refer to TCR and CCR as stress relaxation mechanisms, but in such cases, the CRR mechanism is also implied.

With this wealth of relaxation mechanisms, we can describe the distinctive features for melts of linear and star polymers, as well as star/linear blends where constraint release effects can be important. Upon applying a certain shear rate less than $(\tau_R)^{-1}$, chain retraction can be viewed as an instantaneous process for both the linear matrix and the star arms. Here, we focus on the processes that lead to relaxation of chain orientation. For linear polymers, this includes reptation, TCR, and CLF at low shear rates and CCR at higher shear rates. For star polymers, we have CLF and TCR at low shear rates and CCR at high shear rates. The longest relaxation time for star arm orientation due to CLF, τ_{arm}, is predicted to be [26]

$$\tau_{\mathrm{arm}} = \frac{\pi^3}{2} \tau_e Z_{\mathrm{arm}}^2 \exp\left[\frac{15}{24} Z_{\mathrm{arm}}\right], \qquad (1)$$

where Z_{arm} is the number of entanglements along each star arm. While the numerical factor inside the exponent may change slightly depending on the approximations used, all approaches agree that it is O(1) and this will not be further discussed hereafter.

For star/linear blends, the relaxation mechanisms of the linear chains remain unchanged by the presence of a small fraction of star arms, whereas on the other hand, the stars dynamics is affected by the linear matrix. The orientation of their arms is still primarily relaxed by CLF and TCR, but the nature of these processes is altered when star/linear entanglements are "short-lived" compared to star/star entanglements for blends having span molar mass of the arms similar to that of the linear chains. It is helpful for the subsequent discussion to introduce the concept of "thin tube" and "fat tube" surrounding the star arms [31,40]. The thin tube describes the restriction on lateral motion of the star arm due to entanglement with both other star arms and with the linear matrix molecules. The "fat tube," on the other hand, describes the restriction to lateral motion that remains after all of the star-linear entanglements are removed, leaving only star-star entanglements. Depending on the molar masses of the linear chains and the star arms, the latter may relax at least partially within their fat tubes. For a given star/linear blend, we must then consider whether CLF occurs in the thin tube or the fat tube. The thin tube CLF time, τ_{arm}, is essentially unchanged from the case of pure star polymers (without the linear polymer background but with a number of entanglements equal to the sum of the star-star and star-linear entanglements of the blend). The fat tube CLF time, $\tau_{\mathrm{arm}}^{\mathrm{Fat}}$, can be estimated by accounting for entanglement dilution. First, we replace Z_{arm} by $Z_{S/S} \approx \phi_S Z_{\mathrm{arm}}$, where ϕ_S is the volume fraction of stars and the value of the dilution exponent is taken to be 1 [7,23]. Second, we replace τ_e by τ_e^{CRR}, which is the Rouse time of the thin tube that is envisioned as undergoing Rouse-like fluctuations within the star/star entanglements

(i.e., the fat tube)

$$\tau_e^{\text{CRR}} = \frac{2}{3\pi^2} \tau_{d,\text{lin}} \left[\frac{Z_{\text{arm}}}{Z_{S/S}}\right]^2.$$

When the star polymers are not self-entangled or only weakly self-entangled, $Z_{S/S} \sim 1$, and thus the fat tube CLF time can be derived as $\tau_{\text{arm}}^{\text{Fat}} \approx \tau_e^{\text{CRR}}$. The star arm can be approximated as no longer self-entangled, and consequently, there is no separation between time scales for relaxation and orientation in the fat tube.

The state-of-the-art molecular constitutive model, which describes the structure and stress of entangled linear polymer melts in flow, is the Graham, Likhtman, Milner, and McLeish (GLaMM) model [19]. It has also been adapted for entangled star polymers in a solution by Tezel *et al.* [25], simply by switching-off the terms that describe reptation (GLaMM-R is GLaMM without the inclusion of reptation). Although it might seem at first sight as though the GLaMM-R approach could also be applied for star-linear blends, there is an important potential limitation for adapting GLaMM to mixed architecture blends of monodisperse polymers. The GLaMM model is a description of single-component monodisperse polymer melts, and it is, therefore, not possible to incorporate the thin/fat tube physics that arise from constraints with different characteristic rates of release and renewal. Significant progress has been made toward this end for bidisperse linear/linear blends [12,40,41]. Such considerations would also be necessary in our system at higher concentrations of the star polymer, and we should not expect the GLAMM approach to work in that case, but the generalization to mixed architecture systems remains a challenge. However, we show here that if we limit the system to a range of molar masses and concentrations where there are no star self-entanglements, the star/linear blends can be described within the GLaMM-R framework, which effectively treats the arm relaxation as an apparent one-component star-linear network. For this work, we use the publicly available GLaMM code [19], modified to follow the approach of Tezel *et al.* [25].

In particular, we address the coupling of flow and constraint release with the aim to establish an experimental protocol for identifying component contributions and improving our understanding of nonlinear stress relaxation processes in mixed architecture blends. We combine the existing GLaMM-R model with rheo-small-angle neutron scattering (SANS) in order to measure and predict the structure of star polymers in a star/linear blend in the nonlinear shear flow regime. We choose a star/linear blend for which the star arms are roughly half the size of the surrounding linear chains. In this way, we ensure that both the star and linear polymers share virtually the same Rouse relaxation spectrum within their respective thin tubes. We also chose the blend composition such that the star polymers are weakly self-entangled, hence there is virtually no fat tube around the star arms. The linear viscoelastic properties of similar systems are fairly well understood [7,20], which forms a good basis for investigating the nonlinear flow regime.

Through this systematic investigation, we wish to achieve three goals: (i) reaffirm the predictive power of tube-based models for mixed architecture blends which allow tuning constraint release effects, hence the dynamics; (ii) demonstrate the power of rheo-SANS (simultaneous measurement of bulk rheology and ~~probe~~ microstructure) as a tool uniquely suited for studying nonlinear rheology in mixed architecture blends; (iii) show that whereas the linear viscoelasticity of the examined star/linear polymer blend is hardly distinguishable from that of the linear matrix, rheo-SANS provides distinct signatures of star and linear polymer deformation in flow.

II. MATERIALS AND METHODS

A. Sample preparation

The polymer blend used consisted of a fully protonated polybutadiene (h-PBd) symmetric four-arm star polymer at 10 wt. % in a matrix of fully deuterated linear with weight average molar mass $M_w = 89$ kg/mol and polydispersity $M_w/M_n = 1.08$. The overlap concentration of the star is estimated to be $c^* = 3.42$ wt. % [42]; hence, the star at about $3c^*$ is semidilute albeit not entangled (the estimated entanglement concentration is about 15 wt. % [42]). This mixture provides adequate contrast versus the background of deuterated material and the star is at low enough concentration to avoid phase separation due to isotope effects, which is known to occur in solutions with 35–65 wt. % deuterated materials [43]. The linear and star PBd polymers, with 1,4 rich microstructure [*cis*-1,4, 70%; *trans*-1,4, 23%; and 3, 4, 7% determined from nuclear magnetic resonance (NMR) spectroscopy], were synthesized using high vacuum anionic polymerization techniques. In the case of the four-arm polybutadiene star, an excess of the living polybutadiene ($\sim$30%) was reacted with 1,2-bis (dichloromethylsilyl) ethane (linking agent) in order to drive the reaction to completion. After completion of the reaction, the excess of the linear PBd was removed by repeated fractional precipitation (toluene/MeOH), until highly pure four-arm star PBd was obtained, as monitored by size exclusion chromatography (SEC). All intermediates and final product were analyzed by SEC and NMR. The total molar mass of the final fractionated star was $M_w = 176$ kg/mol with $M_w/M_n = 1.08$ as obtained from SEC with PS standards and appropriate correction for PBd. With this choice of molar masses, both the linear matrix and the star arms are significantly above the entanglement molar mass of 1,4-PBd (2.17 kg/mol, extracted from the fit of the linear PBd data with the Likhtman–McLeish (LM) model, see Sec. III A below). Each blend was made by first dissolving the individual components into good solvent tetrahydrofuran until they were fully dispersed. Then the ingredients were mixed together thoroughly before driving off the solvent. The latter was initially evaporated at room temperature and atmospheric pressure before being subjected to progressively higher vacuum at 30–40 °C. The samples also contained small amounts (0.1 wt. %) of butylated hydroxytoluene antioxidant to reduce the risk of degradation. The polymers were then kept under high vacuum for 24 h before testing, in order to remove any possible remaining solvent.

B. Rheological measurements

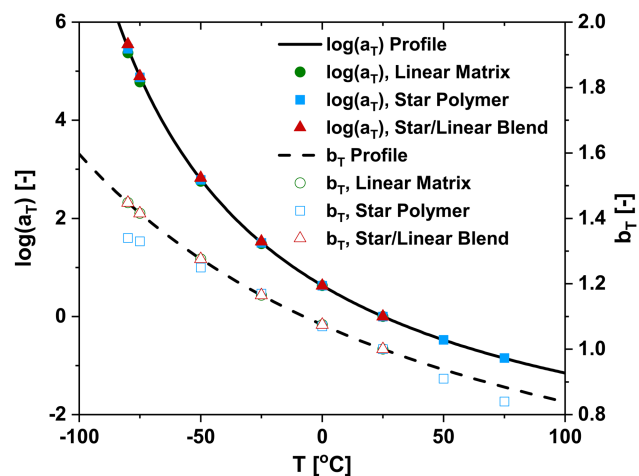Linear viscoelastic measurements were performed with an ARES (TA, USA) strain-controlled rheometer. The rheometer

FIG. 1. The horizontal and vertical shift factors (a_T and b_T, respectively) as functions of the temperature. For the horizontal shift factor, the WLF fit for the pure components and the star/linear blend is also reported (solid black line; $C_1 = 3.92$ and $C_2 = 180 \pm 1$ K). For the vertical shift factor, the calculated vertical shift reflecting the temperature density compensation is also reported (dashed black line; the density was calculated according to the formula $\rho = 1.0547 - 5.6 \times 10^{-4}$ T, where T is the temperature in Kelvin) [33].

is equipped with a 2 K FRTN1 force rebalance transducer, and temperature control ($\pm 0.1\,^\circ$C) is achieved by means of a nitrogen gas convection oven and a liquid nitrogen Dewar. Dynamic oscillatory shear experiments were performed from -75 to $75\,^\circ$C in steps of $25\,^\circ$C. A single measurement was also performed at $-80\,^\circ$C in order to detect the high-frequency crossover of the viscoelastic moduli. The strain amplitude was in the range 2–7%, ensuring measurements in the linear viscoelastic regime at all temperatures investigated. It was ensured that residual stresses due to loading were fully relaxed and the polymer samples were allowed to equilibrate at the test temperature.

Time-temperature superposition was used in order to obtain master-curves at a reference temperature $T_0 = 25\,^\circ$C. The horizontal shift factor a_T is described empirically by the Williams–Landel–Ferry (WLF) [44] equation $\log(a_T) = -C_1(T - T_0)/(C_2 + T - T_0)$, where C_1 and C_2 are material constants that depend on T_0. In our specific case, the polybutadiene was found to have $C_1 = 3.9 \pm 0.1$ and $C_2 = 180 \pm 1$ K as also shown in Fig. 1. The vertical shift factor was $b_T = \rho_0 T_0/(\rho T)$, where ρ is the polymer density and T the absolute temperature (in Kelvin). Its values at different temperatures are of the order of unity. These parameters are comparable to the values reported in the literature [45].

C. Rheo-SANS measurements

The Rheo-SANS measurements were performed at the Manuel Lujan, Jr. Neutron Scattering Center, Los Alamos National Laboratory in Los Alamos, NM, using a specially constructed Couette flow device (CLNR) on the low-q diffractometer beam-line [46]. The scattering vector range $q = 4\pi \sin(\theta/2)/\lambda_N$ covered $2 \times 10^{-2} < q < 1 \times 10^{-1}\,\text{Å}^{-1}$, where the scattering vector was defined by the neutron wavelength λ_N and the scattering angle θ. The 8 mm diameter neutron beam passes through the sample in the radial or shear-gradient

direction and thus probes the polymer conformation along the velocity-vorticity plane.

The Couette device (CLNR) was originally developed as a strain-rate controlled neutron scattering device for studying the behavior of highly viscous systems [46]. Its main features include high torque (up to 200 Nm), high shear rate (900 s^{-1}), and high temperature (over 260 °C) under a nitrogen environment. The CLNR geometry consists of two aluminum concentric cylinders: an inner stationary bob and an outer rotating cup. The inner bob has a diameter of 53.34 mm and has a hollowed core to provide an unimpeded neutron path. The bottom of the bob is machined to have a 1° cone to mitigate edge effects and produce a constant shear across the sample. The gap is small, 0.375 mm, in order to provide a stable Taylor–Couette flow (free of elastic instabilities) well into the nonlinear flow regime. The maximum attainable Weissenberg number prior to instability, Wi^{max}, is calculated from $Wi^{max} = K_{crit}(r_1/d)^{1/2}$, where d is the gap separation, r_1 is the radius of the inner cylinder, and $K_{crit} = 5.92$ [47]. Internally housed heating elements maintained the temperature at 25 °C and an insulating blanket surrounded the apparatus in order to reduce thermal fluctuations. After sample loading, a rest time of about 10 min was allowed for the polymers to reach the set temperature and release residual stresses from loading. Details of the first CLNR prototype are reported in the literature [48]. However, the system used here was redesigned to allow stable flow up to $Wi^{max} = 30$ (based on the linear chain terminal time) and also to reduce the sample volume required to fill the device.

The isotropic SANS data in the absence of shear were reduced to 1D scattering intensity using a radial average. Due to the geometry of the experimental setup, the scattering profiles of the blend in the presence of flow are elongated in the vorticity direction, i.e., perpendicular to the flow direction. The two-dimensional (2D) scattering intensities were calculated using software from the host institute and normalized to the absolute scale via calibration with the incoherent scattering and application of background corrections [46]. The degree of anisotropy in these 2D scattering patterns was characterized by determining a sectorial average of the scattering intensity along the vorticity and flow directions with an opening angle of $\pm 2.5°$ from each axis. The anisotropy ratio was then defined by taking the integrated data $2 \times 10^{-2} < q < 1 \times 10^{-1}\,\text{Å}^{-1}$ and dividing the scattering intensity in the vorticity direction by the data along the flow direction.

The rheo-SANS measurements were used to investigate how the single chain structure factor evolves for the star/linear polymer blend under shear flow in the Couette device. A direct comparison of the experimental data, obtained at different flow rates, was made with the GLaMM-R model.

SANS has been performed by previous investigators for various polymer architectures [2,8,37]. *In situ* SANS of polymeric melts under deformation is of particular interest in studying the relaxation and deformation processes. Recent work has been performed via neutron scattering for a Pouseille geometry, using data taken at several points along a 4:1 contraction, and subsequently, a 1:4 expansion with a recirculating polymer flow [18]. In the present work, the use of a low-curvature Couette geometry simplifies the data analysis in that

changes in the velocity gradient across the gap are small enough that the flow may be approximately modeled as simple shear flow in the plane of interest (in our case, it is the flow/vorticity plane). The capability of the Couette shear cell to operate at high torque and high shear, discussed later in further detail, allows for the investigation of entangled polymeric systems, which are too viscous to be studied in conventional rheometers with this geometry. The blend investigated in this work (10 wt. % four-arm star polybutadiene in 90 wt. % linear deuterated polybutadiene with the same span molecular weight) offers a large operational time-window to study the molecular dynamics of the minority star component by SANS. In particular, our aim is to consider rates of deformation that orient the star polymers but leave the linear matrix mostly relaxed.

III. RESULTS AND DISCUSSION

A. Linear rheology

Figure 2(a) depicts the frequency-dependent storage and loss moduli, G′ and G″, respectively, at a reference temperature of 25 °C as well as the tan(δ) versus shifted frequency. It can be seen that the relaxation process of the pure star polymer is characterized by a broad and smooth peak of G″, followed by a strong decay through the crossover between G′ and G″ at lower frequencies associated with the fluctuations of the arms. On the other hand, the linear chain matrix exhibits a single loss peak (at the moduli crossover), which marks its terminal regime. In the case of the polymer blend, the linear chain dominates the terminal relaxation and there is very little distinction between the linear viscoelastic (LVE) spectra of the linear chain and the blend, with the exception of the low-frequency G′ data. We have confirmed that the data are not an artifact associated with phase angle resolution, hence this small deviation of the blend G′ data marks the effect of star-linear topological coupling which can be also appreciated in the loss angle plot in Fig. 2(b) and are further discussed in the context of the scattering data below. However, over most of the frequency range, it is evident that the dynamic oscillatory measurements are not sensitive enough to clearly separate, at least quantitatively, the contribution of the star polymer from the linear matrix in the polymer blend.

The estimated values for τ_d shown in Fig. 2(a), and also listed in Table I, are based upon the crossing points for the G′ and G″ data. Also shown in Table I are the number of entanglements per chain Z (per arm for the pure star). In the case of the blend, we get $Z_{blend} = \phi_s Z + (1 - \phi_s)Z_{linear} = 45$, considering both star and linear chain entanglements, although only a few entanglements come from the star polymer. Finally, we give the estimated value of the plateau modulus G_e evaluated as the value of G′ corresponding to the minimum of the loss factor, and the estimated values of the Rouse time based upon the measured values of τ_d and the expected relationship $\tau_R = \tau_d/3Z$ for the linear chain, and the approximation, $\tau_{R,Star}(2Z_{arm}) \approx \tau_{R,linear}(Z)/4$. It should be noted that the data entered in Table I for the blend reflects values for the linear chain within the blend. The relaxation for the star in the
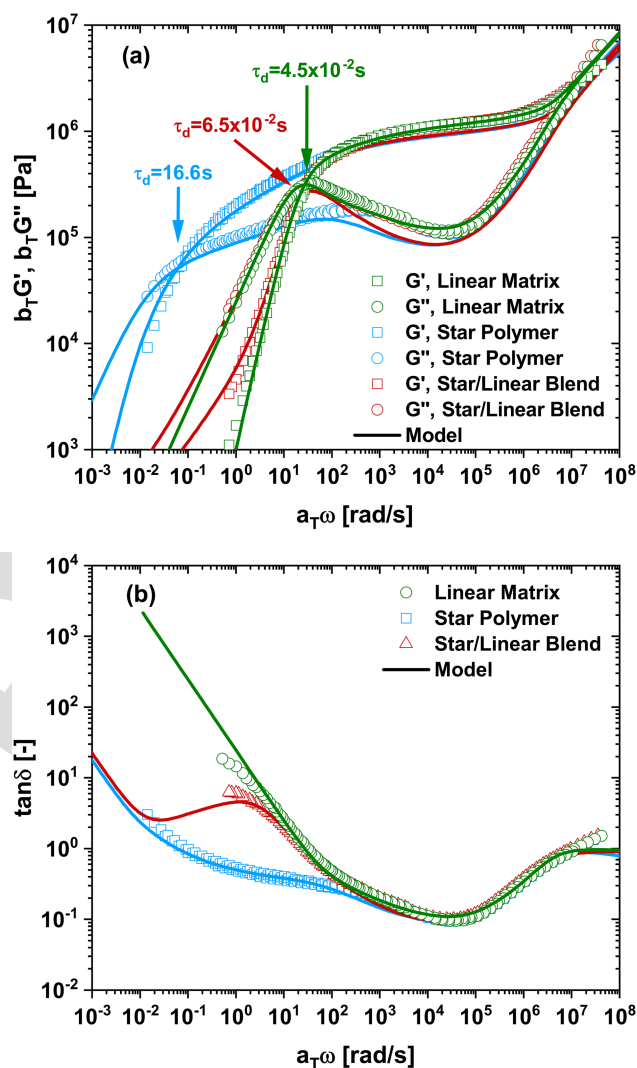

FIG. 2. (a) Linear viscoelastic master-curves (shifted storage and loss moduli versus shifted frequency) of the linear matrix, the star polymer, and the star/linear blend at a reference temperature of 25 °C, along with fits (solid lines) using the tube-based Likhtman–McLeish (LM) model for the linear matrix and the BoB model for the star polymer, and the star/linear polymer blend (see text). The respective characteristic times at the moduli crossover are indicated by arrows. (b) Respective data are represented in the more sensitive plot of tan(δ) versus shifted frequency.

blend cannot be measured directly but can be estimated by means of Eq. (2).

We can also obtain estimates of parameters for the linear chain applying the LM mesoscopic model [14] for the entangled linear polymer, including the characteristic relaxation times. The LM model takes into account CLF, CR, and longitudinal stress relaxation along the tube. The only

TABLE I. Linear viscoelastic parameters of the linear matrix, the star polymer, and the star/linear blend at a reference temperature of 25 °C. The LVE parameters were obtained directly from the data (see text).

	τ_d (s)	Z (–)	τ_R (s)	G_e (MPa)
Linear	4.5×10^{-2}	41	3.7×10^{-4}	
Star	16.6	20	8.7×10^{-5}	1.65
Star/linear blend	6.5×10^{-2}	45	4.8×10^{-4}	1.65

parameters are M_e, G_e, τ_e, and c_ν (constraint release factor). Their values, obtained from a fitting procedure, are $\tau_e = 3.9 \times 10^{-7}$ s, $M_e = 2.17$ kg/mol (from the high-frequency moduli crossover), and $G_e = 1.65$ MPa. This value of M_e corresponds to $Z = 41$ for the linear matrix and $Z_s = 80$ for the entire four-arm star. The model predictions are shown as the solid lines in Fig. 2(a).

Similarly, the generalized tube-based branch-on-branch model (BoB) has been used for analyzing the dynamics of the entangled star polymer and the star/linear blend [15,16] (to this end, the open source program RepTate has been employed). A dilution exponent of 1 has been used for the star polymers and the blend. For the BoB fit of the star/linear blend, we have considered the molecular characteristics of the components presented in Sec. II A above and the same parameters from the LM fit ($\tau_e = 3.9 \times 10^{-7}$ s, $M_e = 2.17$ kg/mol, and $G_e = 1.65$ MPa), with $Z_{\text{blend}} = 45$ for the blend, considering both star and linear chain entanglements. The density value used in BoB is 1450 kg/m^3, making the above G_e and M_e values consistent through the rubber elasticity relationship. The BoB fitting results are also shown in Fig. 2(a). It is evident that the BoB model is able to capture the small low-frequency deviation of G' due to the relaxation of the star polymer in the linear matrix. The loss factor plot of Fig. 2(b) is suggestive of a decoupled two-mode relaxation (linear and star) of the blend; however, the BoB model in the present form may not account entirely correctly for the dilution effect of the linear chain's CLF on the star. In view of this, as well as the lack of experimental data at lower frequencies, definite conclusions about the role of the star cannot be drawn.

Note that the values of the parameters obtained from the LM and BoB model fits are slightly higher than those estimated directly from the experimental data. The latter values are consistent with the literature, where the respective reported values are also slightly lower than those obtained from fitting with the LM model [49,50]. The value of τ_e is consistent with that used by Kapnistos *et al.* [33] and the monomeric friction coefficient of PBd. We shall not explore this further and consistently apply the GLaMM-R model for predicting both rheology and structure of the stars with the same values.

The above analysis of the LVE spectra shows that discriminating between the pure linear matrix and the star/linear blend in the present situation with similar Z_{linear} and Z_{blend} is a subtle issue, hence, complementary evidence from scattering is highly desirable.

Since a direct measurement of the terminal relaxation time of the star component within the blend is not possible given the lack of a distinct feature in the LVE spectrum, we obtained estimates of $\tau_{\text{arm}}^{\text{Fat}}$ (obtained through τ_e^{CRR}). By using $Z_{S/S} = 2$ for our system, we can use Eq. (2) to estimate that $\tau_e^{\text{CRR}} \approx 0.3$ s. It thus follows that $\tau_{\text{arm}}^{\text{Fat}} \approx \tau_e^{\text{CRR}}(Z_{S,S})^2 = 1.2$ s. We recognize the approximate nature of this estimate. Nevertheless, it does suggest that we have approximately one order of magnitude separating the characteristic terminal relaxation time of the star ($\tau_{\text{arm}}^{\text{Fat}}$) and linear ($\tau_{d,\text{lin}}$) polymers, and this provides a reasonable window in terms of shear rate for interrogating the star component in the star/linear polymer blend. In fact, this means that the star arms will fully relax only after the linear matrix has fully relaxed.

A clear message from the linear rheological experiments is that the linear polymer matrix dominates the star/linear polymer blend, hence, the star signature cannot be easily discerned. The rheo-SANS experiment is the most viable alternative tool to uniquely extract the information on the conformational changes and dynamics of the minority component under shear.

B. Rheo-SANS results

In the rheo-SANS measurements, the deformation process is controlled by the applied shear rates, i.e., $\dot{\gamma} = 0$ (equilibrium), 8.1, 16.1, and 24.2 s^{-1} at 25 °C and probed through the scattering patterns. We can use the crude estimate of $\tau_{\text{arm}}^{\text{Fat}}$ to convert these shear rates to Weissenberg numbers, $Wi \approx 9.86$, 19.6, and 29.45, respectively. It should be noted, however, that these values do not appear in the GLaMM calculations and thus they are given here mainly to provide a qualitative frame of reference for estimating the strength of the flow. The use of $\tau_{\text{arm}}^{\text{Fat}}$ is motivated by the fact that our aim is to explore the dynamics of the star polymer in the blend (see also discussion on LVE above). Despite this approximate approach, we note that the Weissenberg number is actually not necessary in our analysis. What is important to appreciate is that the applied rates are lower than the inverse relaxation time of the linear component and larger than the estimated inverse relaxation component of the star component in the blend (see Fig. 2 and Table I) Although we do not perform any direct structural measurement of the linear matrix chains, we expect that they remain virtually unstretched in this range of shear rates, which correspond to Weissenberg numbers based on the terminal time of the pure linear polymer (τ_d in Table I) of 0.36, 0.72 and 1.09, respectively.

The scattering data were collected in the q-range 2×10^{-2}–1×10^{-1} Å^{-1} for 20 min. This chosen time allowed good statistics and at the same time ensured a stable thermal environment. In fact, the two principle limitations of the Couette device are the difficulty to perform experiments below room temperature (six heater cartridges give a good thermal control from room temperature up to 240 °C with small thermal fluctuations ±2 °C) and the difficulty to run experiments under these conditions at steady state for times longer than 45 min.

Therefore, the rheo-SANS procedure to scan and enlarge the investigated q-range [3] was not applicable here. An optimum compromise between short time scales (less than 45 min) and good data statistics (times long enough to have high resolution) was used, and some very interesting structural features were still detectable in the chosen q-range. Due to the experimental conditions, the lowest scattering q-values are missing and thus the chain configuration could not be determined with high precision. Instead, we focused our attention on length scales where chain orientation is accurately determined, i.e., the star arm length scale.

The total intensity scattering in the perpendicular and parallel directions is plotted versus q in Fig. 3. The scattering data have been scaled with the reference length of the tube diameter, which is $a \sim 44$ Å ($q \sim 0.023$ Å^{-1}) as reported in the literature [50]. As can be observed from Fig. 3, the
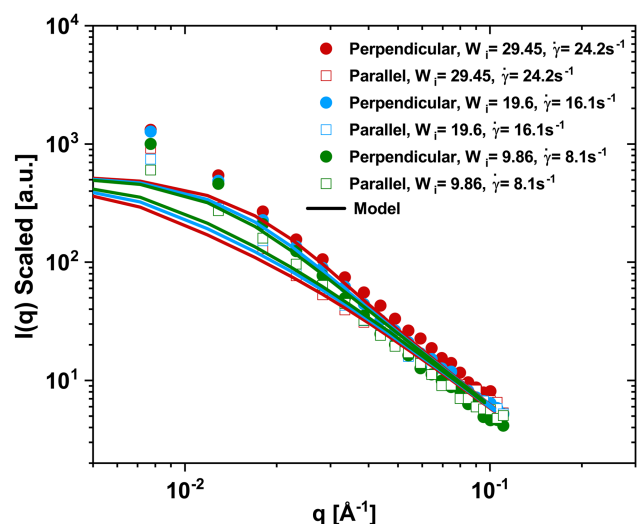
FIG. 3. Experimental 1D perpendicular and parallel components (symbols) versus GLAMM-R calculations (lines).
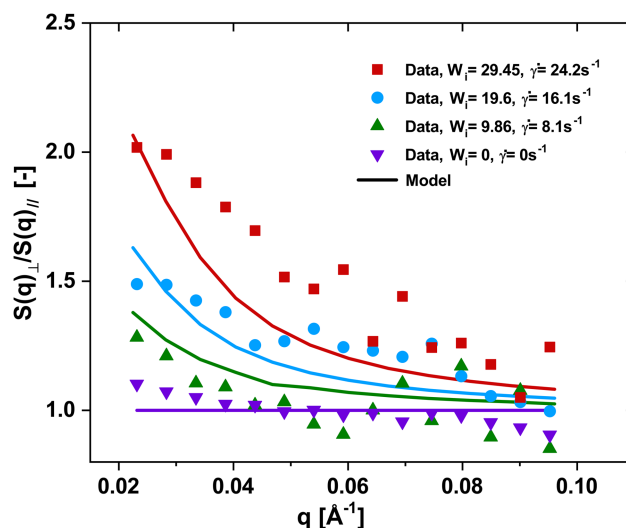

FIG. 4. Plot of the $S(q)\perp/S(q)\|$ (perpendicular-parallel ratio) with SANS data corresponding to Weissenberg numbers of 0, 9.86, 19.6, and 29.45. Lines represent the modified GLaMM-R model predictions (for the isotropic case the line is horizontal through the data). The data used to generate this figure is the same as the data shown in Fig. 3. The maximum experimental uncertainty is 10%.

563 scattering intensity is in good agreement with the predicted
564 values from the GLAMM-R/SANS theory at mid-to-high
565 q-values. However, it fails at low q-values where probably
566 some high-order structuring (nonhomogeneity) as well as the
567 curvature of the Couette cell may contribute.
568   In the original application of the GLAMM-R model for
569 stars in solution, five parameters were needed: three are well-
570 tabulated material properties and two are universal characteris-
571 tic constants for stress relaxation processes. They are G_e, τ_e,
572 and M_e as well as the dimensionless parameters for retraction,
573 c_v, and the constraint release term, R_s. We also need the
574 applied shear rate, $\dot{\gamma}$. The first three parameters are obtained
575 from LVE. The other two parameters, c_v and R_s, are universal
576 constants associated with constraint release (CCR and TCR)
577 and chain retraction [18,19]. Recommended values for these
578 constants can be found in the literature, $c_v = 0.1$, $R_s = 1$ and
579 were selected based on an extensive comparison with experi-
580 mental data [18,19,25]. Finally, the shear rate can be deter-
581 mined directly from the experimental protocol. In our
582 predictions with the GLaMM-R model, we have used $Z = 20$
583 for the probe chain. We recall that the probe chain (star
584 polymer) is surrounded by and entangled with the matrix
585 (linear polymer) in a semidilute regime. Although the neutron
586 scattering investigation is focused on the star polymer behavior,
587 the contribution of the linear matrix is yet present and implicit.
588   In our previous works [2,3], with data over a larger
589 q-region (i.e., lower q-values corresponding to the radius of
590 gyration, R_g), we used the ratio of the scattering intensity
591 along the perpendicular (vorticity) and parallel (velocity)
592 directions, $S(q)\perp/S(q)\|$ as a simple metric of microstructural
593 anisotropy at varying q. With this anisotropy metric, we con-
594 sistently find a q for which star arm anisotropy is maximized.
595 Again, a comparison with the modified GLaMM-R model is
596 possible in the q-range where the orientation of the probe
597 chain is observed. Indeed, in Fig. 4, the ratio $S(q)\perp/S(q)\|$ at
598 different Weissenberg numbers distinguishes between
599 deformed and undeformed configurations. This provides a
600 measure of the degree of deformation (in terms of chain ori-
601 entation) for a range of length scales $2\pi/q$ along the star arm.

602   The isotropic data ($\dot{\gamma} = 0$) shows a very small, nearly neg-
603 ligible upturn at the lowest q-values; this might be due to
604 some parasitic forward scattering for $q < 1/R_g$ or residual
605 voids (air) after the loading process. We note, however, that
606 the SANS experiments were performed after a rest time
607 longer than $10\tau_{d,linear}$, as discussed above.
608   To better appreciate the response of the star in the studied
609 star-linear system (10 wt. % star with $Z = 20$ and 90 wt. %
610 linear), we compare the calculated $S(q)\perp/S(q)\|$ ratio from
611 GLAMM-R with the respective scattering response of a
612 linear polymer mixture (10 wt. % linear with $Z = 20$ and
613 90 wt. % linear) based on GLAMM. The results are shown in
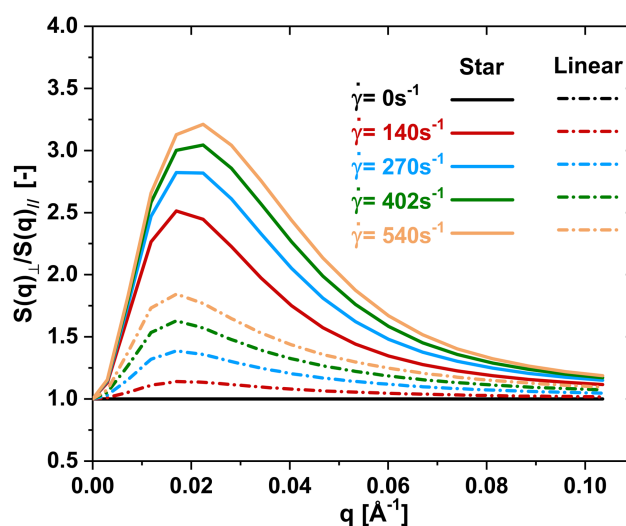614 Fig. 5, where we have selected arbitrary values of the shear

FIG. 5. GLAMM-based calculations of $S(q)\perp/S(q)\|$ for star (solid lines) and linear (dashed-dotted lines) polymers with $Z = 20$, using GLAMM-R (10 wt. % star with $Z = 20$ and 90 wt. % linear) and GLAMM (10 wt. % linear with $Z = 20$ and 90 wt. % linear) models, respectively.

rat $\boxed{12}$, 270, 402, and 540 s^{-1} (at lower rates the anisotropy of the linear chain would overlay on the isotropic profile). Due to the branching nature of the star polymer (and the omission of reptation in GLAMM-R), the anisotropy of the star is more than twice larger (note the higher peak and broader shape of the scattering curves representing the q-dependent S(q)⊥/S(q)∥ ratio). It is clear from these results that while the star-modified GLAMM model is not fully capable of capturing the anisotropy of the scattering data in Fig. 4, it does much better than a linear chain prediction. A further comparison between the GLaMM-R modeling and experimental data is shown in Fig. 6, where 2D scattering contours of the scattering intensities are reported. In the investigated system, the applied flow causes the probed star polymer arm to orient in the flow direction. As mentioned above, at the shear rates considered here, the linear matrix is almost completely relaxed and thus the anisotropic 2D scattering patterns show that the star polymer is weakly oriented along the velocity direction. The measured profiles in the 2D-detector plane are in good qualitative agreement with the calculated results obtained via the GLaMM-R model.

The isointensity contours of 2D anisotropic patterns show a transition from circular (isotropic) to a more ellipsoidal (anisotropic) shape with the increasing rate of deformation (see Fig. 6).

The details of the full scattering pattern provide a more complete picture of chain orientation and deformation than the simple ratio S(q)⊥/S(q)∥ presented in Fig. 4. At zero shear rate, we obtain the well-defined isotropic pattern, possessing a q-invariant value of the scattering ratio S(q)⊥/S(q)∥ = 1 and a perfectly circular 2D profile, as reported in Figs. 4 and 6, respectively. At an applied shear rate of 8.1 s^{-1} (*Wi* = 9.86), a weak anisotropy is observed, highlighted by a smooth leveling-off from the isotropic profile (see Fig. 4). In this region, GLaMM-R provides a good description of the data accounting for the previously mentioned assumption. Further, at 16.1 s^{-1} (*Wi* = 19.6), we still observe an increased anisotropic behavior and GLaMM-R predicts fairly well the scattering pattern. Finally, at the highest applied rate of 24.2 s^{-1} (*Wi* = 29.45), the trend is still qualitatively consistent with the previous shear rates in the scattering event and the anisotropy increases even more, but the GLAMM-R model now seems to underestimate the anisotropy as also seen earlier in Fig. 4. The reason is that the complex star-linear polymer coupling is not considered in the current formulation of one-component system with a simple CCR term. Higher anisotropy with strong appearance of lozenge-shaped scattering patterns (which can be barely evidenced at the low-q regime of the highest rate in Fig. 6) are expected to appear over a wide q-range at much higher shear rates exceeding 100 s^{-1} (not accessible in the present experiment).

IV. CONCLUSIONS

With a combined experimental (rheo-SANS) and modeling (GLaMM-R) approach, we probed the structural change of stars immersed in a linear polymer matrix that had the same molar mass as the sum of two arms and was being sheared at moderate shear rates ($8.1 < \dot{\gamma} < 24.2$ s^{-1}) between the inverse relaxation times of the linear and star components of the blend. The respective range of approximate Weissenberg numbers was $9.86 < \mathrm{Wi} < 29.45$, based on the estimated value of $\tau_{\mathrm{arm}}^{\mathrm{Fat}}$. While the star contribution is barely perceptible in the linear viscoelastic spectrum at low frequencies, their structural anisotropy when weakly sheared is clearly evident in the SANS data, albeit the effect is small. The orientation of the star polymer in the flow is clearly observed in 2D anisotropic patterns. At this time scale, the star-star entanglements are effectively absent, and thus can be neglected in the treatment of the molecular mechanism of the star relaxation. The neutron scattering experiments allowed precise discrimination of the probe star microscopic behavior in the transition from linear to nonlinear regime.

Finally, this work shows that the combination of rheology and neutron scattering is uniquely capable for selectively probing the nonlinear configurations of branched polymers in a bimodal polymer mixture. This protocol is particularly useful for architectural blends and can be extensively applied to other modes of deformation (e.g., extensional) in order to obtain the material's full response to deformation. A more detailed theoretical approach may still be needed for fully interpreting the linear chain contribution in these bimodal polymer melts. Nevertheless, the present set of approximations works well for moderate deformation rates but would not be expected to describe polymer-melt behavior subjected to stronger strain fields. Here, we have provided a platform that can be expanded upon in future works to develop more robust models.
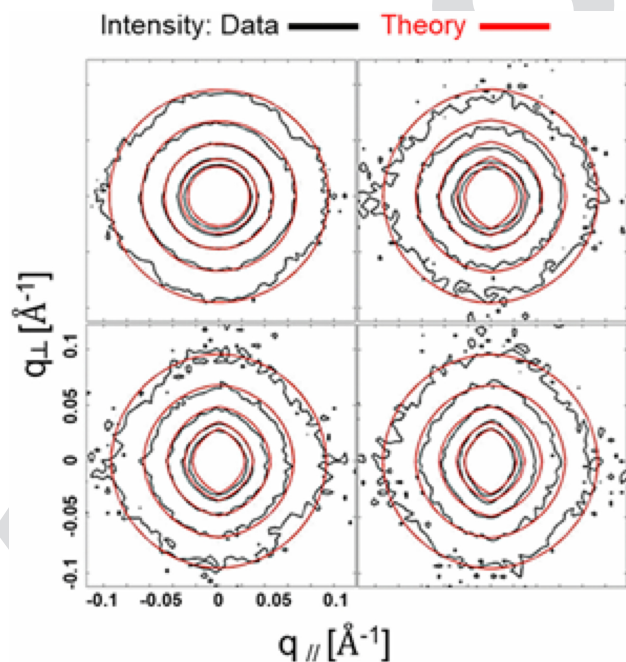

FIG. 6. Experimental (black lines) and modeled (red lines) 2D scattering intensities in the vorticity-velocity plane of the star/linear polymer blend corresponding to applied shear rates of 0 (top left), 8.1 s^{-1} (top right), 16.1 s^{-1} (bottom left), and 24.2 s^{-1} (bottom right). The calculations were performed in the $2 \times 10^{-2} < q < 1 \times 10^{-1}$ Å^{-1} range. The 2D q⊥ and q∥ ranges reported are between -1×10^{-1} and 1×10^{-1}. The deformation direction is horizontal.

Q5
Q6

REFERENCES

[1] Graham, R. S., and T. C. B. McLeish, "Emerging applications for models of molecular rheology," J. Non-Newton. Fluid Mech. **150**, 11–18 (2008).

[2] Ruocco, N., L. Dahbi, P. Driva, N. Hadjichristidis, J. Allgaier, A. Radulescu, M. Sharp, P. Lindner, E. Straube, W. Pyckhout-Hintzen, and D. Richter, "Microscopic relaxation processes in branched-linear polymer blends by Rheo-SANS," Macromolecules **46**, 9122–9133 (2013).

[3] Ruocco, N., D. Auhl, C. Bailly, P. Lindner, W. Pyckhout-Hintzen, A. Wischnewski, L. G. Leal, N. Hadjichristidis, and D. Richter, "Branch point withdrawal in elongational startup flow by time-resolved small angle neutron scattering," Macromolecules **49**, 4330–4339 (2016).

[4] Read, D. J., D. Auhl, C. Das, J. den Doelder, M. Kapnistos, I. Vittorias, and T. C. B. McLeish, "Linking models of polymerization and dynamics to predict branched polymer structure and flow," Science **333**, 1871–1874 (2011).

[5] Shivokhin, M. E., E. van Ruymbeke, C. Bailly, D. Kouloumasis, N. Hadjichristidis, and A. E. Likhtman, "Understanding constraint release in star/linear polymer blends," Macromolecules **47**, 2451–2463 (2014).

[6] Pyckhout-Hintzen, W., A. Wischnewski, and D. Richter, "Mixtures of polymer architectures: Probing the structure and dynamics with neutron scattering," Polymer **105**, 378–392 (2016).

[7] van Ruymbeke, E., S. Coppola, L. Balacca, S. Righi, and D. Vlassopoulos, "Decoding the viscoelastic response of polydisperse star/linear polymer blends," J. Rheol. **54**, 507–538 (2010).

[8] Desai, P. S., B. G. Kang, M. Katzarova, R. Hall, Q. Huang, S. Lee, M. Shivokhin, T. Chang, D. C. Venerus, J. Mays, J. D. Schieber, and R. G. Larson, "Challenging tube and slip-link models: Predicting the linear rheology of blends of well-characterized star and linear 1,4-polybutadienes," Macromolecules **49** (13), 4964–4977 (2016).

[9] Ebrahimi, T., H. Taghipour, D. Grießl, P. Mehrkhodavandi, S. G. Hatzikiriakos, and E. van Ruymbeke, "Binary blends of entangled star and linear poly(hydroxybutyrate): Effect of constraint release and dynamic tube dilation," Macromolecules **50**, 2535–2546 (2017).

[10] Lentzakis, H., S. Costanzo, D. Vlassopoulos, R. H. Colby, D. J. Read, and E. van Ruymbeke, "Constraint release mechanisms for H-polymers moving in linear matrices of varying molar masses," Macromolecules **52**, 3010–3028 (2019).

[11] Hall, R., P. S. Desai, B. G. Kang, Q. Huang, S. Lee, T. Chang, D. C. Venerus, J. Mays, K. Ntetsikas, G. Polymeropoulos, N. Hadjichristidis, and R. G. Larson, "Assessing the range of validity of current tube models through analysis of a comprehensive set of star-linear 1,4-polybutadiene polymer blends," Macromolecules **52**, 7831–7846 (2019).

[12] Graham, R. S., J. Bent, N. Clarke, L. R. Hutchings, R. W. Richards, T. Gough, D. M. Hoyle, O. G. Harlen, I. Grillo, D. Auhl, and T. C. B. McLeish, "The long-chain dynamics in a model homopolymer blend under strong flow: Small-angle neutron scattering and theory," Soft Matter **5**, 2383–2389 (2009).

[13] Lentzakis, H., D. Vlassopoulos, D. J. Read, H. Lee, and T. Chang, "Uniaxial extensional rheology of well-characterized comb polymers," J. Rheol. **57**, 605–625 (2013).

[14] Likhtman, A., and T. C. B. McLeish, "Quantitative theory for linear dynamics of linear entangled polymers," Macromolecules **35**, 6332–6343 (2002).

[15] Das, C., N. J. Inkson, D. J. Read, M. A. Kelmanson, and T. C. B. McLeish, "Computational linear rheology of general branch-on-branch polymers," J. Rheol. **50**, 207–234 (2006).

[16] Das, C., D. J. Read, D. Auhl, M. Kapnistos, J. den Doelder, I. Vittorias, and T. C. B. McLeish, "Numerical prediction of nonlinear rheology of branched polymer melts," J. Rheol. **58**, 737–757 (2014).

[17] Milner, S. T., T. C. B. McLeish, R. N. Young, A. Hakiki, and J. M. Johnson, "Dynamic dilution, constraint-release, and star–linear blends," Macromolecules **31**, 9345–9353 (1998).

[18] Graham, R. S., J. Bent, L. R. Hutchings, R. W. Richards, D. J. Groves, J. Embery, T. M. Nicholson, T. C. B. McLeish, A. E. Likhtman, O. G. Harlen, D. J. Read, T. Gough, R. Spares, P. D. Coates, and I. Grillo, "Measuring and predicting the dynamics of linear monodisperse entangled polymers in rapid flow through an abrupt contraction. A small angle neutron scattering study," Macromolecules **39**, 2700–2709 (2006).

[19] Graham, R. S., A. E. Likhtman, T. C. B. McLeish, and S. T. Milner, "Microscopic theory of linear entangled polymer chains under rapid deformation including chain stretch and convective constraint release," J. Rheol. **47**, 1171–1200 (2003).

[20] van Ruymbeke, E., R. Keunings, and C. Bailly, "Prediction of linear viscoelastic properties for polydisperse mixtures of entangled star and linear polymers: Modified tube based model and comparison with experimental results," J. Non-Newton. Fluid Mech. **128**, 7–22 (2005).

[21] Qin, J., and S. T. Milner, "Tube diameter of oriented and stretched polymer melts," Macromolecules **46**, 1659–1672 (2013).

[22] Bick, D. K., and T. C. B. McLeish, "Topological contributions to nonlinear elasticity in branched polymers," Phys. Rev. Lett. **76**, 2587–2590 (1996).

[23] Kapnistos, M., K. M. Kirkwood, J. Ramirez, D. Vlassopoulos, and L. G. Leal, "Nonlinear rheology of model comb polymers," J. Rheol. **53**, 1133–1153 (2009).

[24] Marrucci, G., "Dynamics of entanglements: A nonlinear model consistent with the Cox-Merz rule," J. Non-Newton. Fluid Mech. **62**, 279–289 (1996).

[25] Tezel, A. K., J. P. Oberhauser, R. S. Graham, K. Jagannathan, T. C. B. McLeish, and L. G. Leal, "The nonlinear response of entangled star polymers to start-up of shear flow," J. Rheol. **53**, 1193–1214 (2009).

[26] McLeish, T. C. B., "Tube theory of entangled polymer dynamics," Adv. Phys. **51**, 1379–1527 (2002).

[27] Watanabe, H., "Viscoelasticity and dynamics of entangled polymers," Prog. Polym. Sci. **24**, 1253–1403 (1999).

[28] Doi, M., and S. Edwards, *The Theory of Polymer Dynamics* (Oxford University, New York, 1989).

[29] de Gennes, P. G., *Scaling Concepts in Polymer Physics* (Cornell University, New York, 1979).

[30] Milner, S. T., T. C. B. McLeish, and A. E. Likhtman, "Microscopic theory of convective constraint release," J. Rheol. **45**, 539–563 (2001).

[31] Auhl, D., P. Chambon, T. C. B. McLeish, and D. J. Read, "Elongational flow of blends of long and short polymers: Effective stretch relaxation time," Phys. Rev. Lett. **103**, 136001 (2009).

[32] van Ruymbeke, E., Y. Masubuchi, and H. Watanabe, "Effective value of the dynamic dilution exponent in bidisperse linear polymers: From 1 to 4/3," Macromolecules **45**, 2085–2098 (2012).

[33] Kapnistos, M., D. Vlassopoulos, J. Roovers, and L. G. Leal, "Linear rheology of architecturally complex macromolecules: Comb polymers with linear backbones," Macromolecules **38**, 7852–7862 (2005).

[34] Kirkwood, K. M., L. G. Leal, D. Vlassopoulos, P. Driva, and N. Hadjichristidis, "Stress relaxation of comb polymers with short branches," Macromolecules **42**, 9592–9608 (2009).

[35] Tezel, A. K., L. G. Leal, and T. C. B. McLeish, "Rheo-optical evidence of CCR in an entangled four-arm star," Macromolecules **38**, 1451–1455 (2005).

[36] Tezel, A. K., and L. G. Leal, "Shear rheology of asymmetric star polymers," Macromolecules **39**, 4605–4614 (2006).

[37] Blanchard, A., R. S. Graham, M. Heinrich, W. Pyckhout-Hintzen, D. Richter, A. E. Likhtman, T. C. B. McLeish, D. J. Read, E. Straube, and J. Kohlbrecher, "Small angle neutron scattering observation of chain retraction after a large step deformation," Phys. Rev. Lett. **95**, 166001 (2005).

[38] Ianniruberto, G., and G. Marrucci, "Convective orientational renewal in entangled polymers," J. Non-newton. Fluid Mech. **95**, 363–374 (2000).

[39] Ianniruberto, G., and G. Marrucci, "Convective constraint release (CCR) revisited," J. Rheol. **58**, 89–102 (2014).

[40] Read, D. J., K. Jagannathan, S. K. Sukumaran, and D. Auhl, "A full-chain constitutive model for bidisperse blends of linear polymers," J. Rheol. **56**, 823–873 (2012).

[41] Boudara, V. A. H., J. D. Peterson, L. G. Leal, and D. J. Read, "Nonlinear rheology of polydisperse blends of entangled linear polymers: Rolie-Double-Poly models," J. Rheol. **63**, 71–91 (2019).

[42] Rubinstein, M., and R. H. Colby, *Polymer Physics (Chemistry)* (Oxford University, New York, 2003).

[43] Bates, F. S., G. D. Wignall, and W. C. Koehler, "Critical behavior of binary liquid mixtures of deuterated and protonated," Phys. Rev. Lett. **55**, 2425–2428 (1985).

[44] Ferry, J. D., *Viscoelastic Properties of Polymers* (Wiley, New York, 1961).

[45] Park, S. J., P. S. Desai, X. Chen, and R. G. Larson, "Universal relaxation behavior of entangled 1,4-polybutadiene melts in the transition. Frequency range," Macromolecules **48**, 4122–4131 (2015).

[46] Hjelm, R. P., "The resolution of TOF low-Q diffractometers: Instrumental, data acquisition and reduction factors," J. Appl. Cryst. **21**, 618–628 (1988).

[47] Pakdel, P., and G. H. McKinley, "Elastic instability and curved streamlines," Phys. Rev. Lett. **77**, 2459–2462 (1996).

[48] Yearley, E. J., L. A. Sasa, C. F. Welch, M. A. Taylor, K. M. Kupcho, R. D. Gilbertson, and R. P. Hjelm, "The Couette configuration of the Los Alamos Neutron Science Center neutron rheometer for the investigation of polymers in the bulk via small-angle neutron scattering," Rev. Sci. Instrum. **81**, 045109 (2010).

[49] Graessley, W. W., *Polymer Liquids and Networks: Dynamics and Rheology* (Garland Science, New York, 2008).

[50] Fetters, L. J., D. J. Lohse, D. Richter, T. A. Witten, and A. Zirkelt, "Connection between polymer molecular weight, density, chain dimensions, and melt viscoelastic properties," Macromolecules **27**, 4639–4647 (1994).